Author(s): Erkkilä, Anna-Leena; Leppänen, Teemu; Hämäläinen, Jari; Tuovinen, Tero

Title: Hygro-elasto-plastic model for planar orthotropic material

Year: 2015

Version:

Please cite the original version:

Erkkilä, A.-L., Leppänen, T., Hämäläinen, J., & Tuovinen, T. (2015). Hygro-elasto-plastic model for planar orthotropic material. International Journal of Solids and Structures, 62, 66-80. https://doi.org/10.1016/j.ijsolstr.2015.02.001

International Journal of Solids and Structures 62 (2015) 66–80

Contents lists available at ScienceDirect

International Journal of Solids and Structures

journal homepage: www.elsevier.com/locate/ijsolstr

Hygro-elasto-plastic model for planar orthotropic material

Anna-Leena Erkkilä [a,*], Teemu Leppänen [b], Jari Hämäläinen [a], Tero Tuovinen [c]

[a] Lappeenranta University of Technology, PO Box 20, FI-53851 Lappeenranta, Finland
[b] LUT Savo Sustainable Technologies, Lappeenranta University of Technology, Varkaus unit, Osmajoentie 75, FI-78210 Varkaus, Finland
[c] University of Jyväskylä, PO Box 35, FI-40014 Jyväskylä, Finland

ARTICLE INFO

Article history:
Received 17 October 2014
Received in revised form 28 January 2015
Available online 17 February 2015

Keywords:
Paper
Elasto-plasticity
Hygroexpansivity
Shrinkage
Anisotropy
Dry solids content
Buckling

ABSTRACT

An in-plane elasto-plastic material model and a hygroexpansivity-shrinkage model for paper and board are introduced in this paper. The input parameters for both models are fiber orientation anisotropy and dry solids content. These two models, based on experimental results, could be used in an analytical approach to estimate, for example, plastic strain and shrinkage in simple one-dimensional cases, but for studies of the combined and more complicated effects of hygro-elasto-plastic behavior, a numerical finite element model was constructed. The finite element approach also offered possibilities for studying different structural variations of an orthotropic sheet as well as buckling behavior and internal stress situations under local strain differences. A few examples are presented of the effect of the anisotropy and moisture streaks under stretching and drying conditions on strain differences and buckling. The internal stresses were studied through a case in which the drying of different layers occurred at different stages. Both the anisotropy and moisture streaks were capable of rendering the buckling of the sample visible. The permanency of these defects highly depends on several process stages and tension conditions of the sheet, as demonstrated in this paper. The application possibilities of the hygro-elasto-plastic model are diverse, including investigation into several phenomena and defects appearing in drying, converting and printing process conditions.

1. Introduction

Paper and board have elasto-visco-plastic properties, exhibiting such rheological behaviors as delayed strain recovery, stress relaxation and creep (Skowronski and Robertson, 1986; Rance, 1956; Steenberg, 1947; Gates and Kenworthy, 1963; Lyne and Gallay, 1954). The hygroscopic nature of the pulp fibers causes dimensional changes in the paper or the board when subject to influences of humidity changes or treatments which involve water intake or drying (Rance, 1954; Page and Tydeman, 1962; Uesaka, 1994; Nanko and Wu, 1995). Shrinkage during drying (Wahlström and Lif, 2003; Hoole et al., 1999; Nanri and Uesaka, 1993; Kiyoaki, 1987) and hygro- and hydroexpansivity (Uesaka, 1991; Salmen et al., 1987; Larsson and Wagberg, 2008; Lif et al., 1995; Mendes et al., 2011) are widely studied components of sorption based dimensional instabilities. Natural fibers and their treatments, bonds between fibers and their orientation in the fiber network, additives and manufacturing conditions all affect dimensional instability and mechanical properties of paper or board (Silvy, 1971; Wahlström and Fellers, 2000; Alava and Niskanen, 2006; Kouko et al., 2007; Nordman, 1958; Fahey and Chilson, 1963; Salmen et al., 1987; Uesaka et al., 1992; Uesaka and Qi, 1994; Mäkelä, 2009; Lyne et al., 1996; de Ruvo et al., 1976; Manninen et al., 2011; Setterholm and Kuenzi, 1970; Glynn et al., 1961; Leppänen et al., 2008).

Several models to predict in-plane mechanical and rheological properties, shrinkage and hygroexpansivity have been introduced in the literature. Johnson and Urbanik (1984) and Johnson and Urbanik (1987) have provided a nonlinear elastic model to study material behavior in stretching, bending and buckling of axially loaded paperboard plates. Nonlinear elastic biaxial failure criteria have been studied by Suhling et al. (1985) and Fellers et al. (1983). In-plane orthotropic elasto-plastic approaches to estimate the tensile response and deformation of paper have been presented by Castro and Ostoja-Starzewski (2003), Mäkelä and Östlund (2003) and Xia et al. (2002). Viscoelastic models have been used extensively in studying creep or relaxation behavior (Brezinski, 1956; Lif et al., 1999; Lu and Carlsson, 2001; Pecht et al., 1984; Pecht and Johnson, 1985; Rand, 1995; Uesaka et al., 1980).

A formula for the hygroexpansion of paper relating to the hygroexpansion of a single fiber and the efficiency of the stress transfer between fibers has been derived by Uesaka (1994). The traditional theory of linear thermoelasticity was applied to

* Corresponding author. Tel.: +358 40 848 8526; fax: +358 5 411 7201.
E-mail address: anlejoer@gmail.com (A.-L. Erkkilä).

http://dx.doi.org/10.1016/j.ijsolstr.2015.02.001
0020-7683/

estimate hygroexpansion strains in the study of Lavrykov et al. (2004). Hygro-viscoelastic models have been applied to estimate history dependent dimensional stability and hygroexpansivity by Uesaka et al. (1989), Uesaka (1991), Lif et al. (2005) and Lif (2006). Mechano-sorptive creep has been studied, for example, by Urbanik (1995), Strömbro and Gudmundson (2008), Alfthan (2004) and Haslach (1994). Shrinkage profiles have been modeled by Wahlström et al. (1999) and Constantino et al. (2005). The measured moisture dependency of material constants has been employed within the nonlinear elastic model for an investigation of the effect of moisture on mechanical behavior by Yeh et al. (1991). Hygroscopic out-of-plane deformations, such as curling and buckling, have been studied, using elastic constitutive models, by Bloom and Coffin (2000), Leppänen et al. (2005) and Kulachenko et al. (2005); while an elasto-plastic model has been introduced in Lipponen et al. (2008, 2009). The hygroexpansion coefficients are independent of moisture content in these models.

In this paper, an in-plane elasto-plastic material model and a hygroexpansivity-shrinkage model that are functions of the dry solids content and fiber orientation anisotropy index are introduced. The elasto-plastic model is based on fittings of the uni-axial stress–strain curves presented by Lipponen et al. (2008) and Erkkilä et al. (2013). The dependency of the dry paper hygroexpansion coefficient on the anisotropy index was determined using the measurement results presented in Erkkilä et al. (submitted for publication). The drying shrinkage strain as a function of the dry solids content was constructed with an exponential formula based on the measurements provided by Ivarsson (1954), Kijima and Yamakawa (1978) and Tydeman et al. (1966) and summarized by Wahlström et al. (1999) and Wahlström (2004). The relation between the hygroexpansivity and the solids content was derived from the drying shrinkage strain function. Usually, the hygroexpansivity has been considered to be constant (i.e. independent of the moisture content level), which estimates the change in dimensions of a dry paper subject to the relative humidity change. However, in this paper, the dry solids content dependent hygroexpansivity, over the entire range from wet to dry, has been introduced. These two models, the elasto-plastic material model and the hygroexpansivity-shrinkage model, were exploited when numerical solutions were obtained with the finite element method. The use of the anisotropy index instead of that of traditional fiber orientation anisotropy simplified the handling of different in-plane directions in the case of the anisotropic sheet and, for instance, the determination of Hill's yield surface for the finite element approach is straightforward. Analytical one-dimensional solutions were used to estimate plastic and hygroscopic strains in simple cases and the results were compared with numerical simulations.

2. Models

In this section, the one-dimensional elasto-plastic material model (Section 2.1) and the hygroexpansivity-shrinkage model (Section 2.2) are presented. The continuum mechanical model is constructed in Section 2.3 and the numerical solution approach is described in Section 2.4.

2.1. Elasto-plasticity

The stress–strain measurements, used here as the basic data for constructing the material model, were presented in Lipponen et al. (2008) and Erkkilä et al. (2013). The stress–strain curve fittings for the determination of the elastic modulus, yield strain, yield stress and function for the strain hardening behavior were discussed in detail in Erkkilä et al. (2013). The following equation was considered suitable for describing all the uniaxial stress–strain relationships studied:

$$\sigma = \begin{cases} E\varepsilon & \text{if } \varepsilon \leqslant \varepsilon_y \\ E\varepsilon_y - \frac{H}{2E} + \sqrt{H\left(\frac{H}{4E^2} + \varepsilon - \varepsilon_y\right)} & \text{if } \varepsilon > \varepsilon_y \end{cases} \tag{1}$$

where σ is the stress and ε is the strain; the elastic modulus E, the yield strain ε_y and the hardening constant H are the fitting parameters. The fitting parameters were determined for different dry solids contents (R_{sc}) and anisotropy index (ϕ) levels from the materials measured in Erkkilä et al. (2013). To construct the material model, the following equation was used to fit the parameters σ_y, ε_y and H as functions of R_{sc} and ϕ:

$$P = (A_1 + A_2\phi + A_3 R_{sc})^{1/n} \quad P = \{\sigma_y, \varepsilon_y, H\} \tag{2}$$

where A_1, A_2, A_3 and n are the fitting constants listed in Table 1. In Erkkilä et al. (2013) the anisotropy index was defined as:

$$\phi = \sqrt{\frac{1-\xi^2}{\xi + \tan^2\gamma/\xi} + \xi} \tag{3}$$

where ξ is the fiber orientation anisotropy and γ is the angle from the minor axis of the fiber orientation distribution. The anisotropy index in the main direction and cross direction (direction perpendicular to the main direction) obtain values of $\sqrt{\xi}$ and $1/\sqrt{\xi}$, respectively. Table 1 also includes the coefficient of determination r^2 values between the measured parameters from Erkkilä et al. (2013) and their estimates according to Eq. (2). The elastic modulus is determined by $E = \sigma_y/\epsilon_y$, with $r^2 = 0.985$. The material model parameters as a function of ϕ and R_{sc} are presented in Fig. 1. Since the functions fitted according Eq. (2) behave monotonically a reasonable amount of extrapolation is permitted. This may be needed, for example, if the local variation of the fiber orientation is considered. The model has a lower limit for solids content; i.e., it is valid if $R_{sc} > 0.3$; the parenthetical expression of Eq. (2) reaches negative values for yield stress σ_y with low solids content if the anisotropy index is also simultaneously low. The material model can be used directly to calculate the material parameters of the orthotropic sample in any in-plane direction or at any solids content level. Examples of the determination of plastic strain as a consequence of stretching either 0.3% or 1% and releasing afterwards are presented in Fig. 2.

2.2. Hygroexpansivity and shrinkage

The hygroexpansivity-shrinkage model is based on the measured relationships between the dry paper hygroexpansivity β_d and anisotropy index ϕ

$$\beta_d = k\phi^{\nu} \tag{4}$$

and between the drying strain ε_{ds} and the dry paper hygroexpansivity

$$\varepsilon_{ds} = -\frac{1}{a}\beta_d + \frac{b}{a} \tag{5}$$

where k, ν, a and b are fitted constants for freely-dried (fd) and restraint-dried (rd) samples made of either softwood pulp (SW), thermomechanical pulp (TMP) or a mixture of those (MIX); see

Table 1
The fitting parameters of Eq. (2) and the coefficients of determination r^2 for the yield stress σ_y, the yield strain ε_y and the hardening constant H.

	A_1	A_2	A_3	n	r^2
σ_y	−5.9030 (Pa^n)	3.1959 (Pa^n)	18.3077 (Pa^n)	0.1760 (–)	0.965
ε_y	380.4181 (–)	14.3408 (-)	−269.8327 (–)	−0.7720 (–)	0.816
H	−0.6021 (Pa^{2n})	4.0423 (Pa^{2n})	11.3795 (Pa^{2n})	0.0715 (–)	0.890

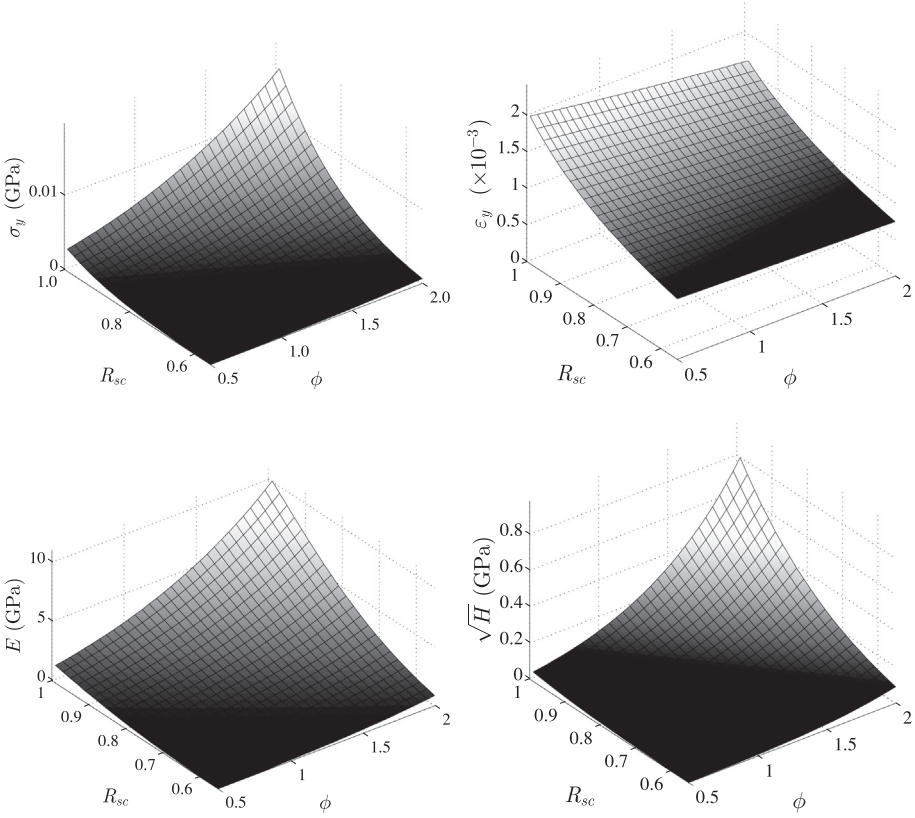

Fig. 1. Material parameters as a function of the anisotropy index ϕ and solids content R_{sc}.

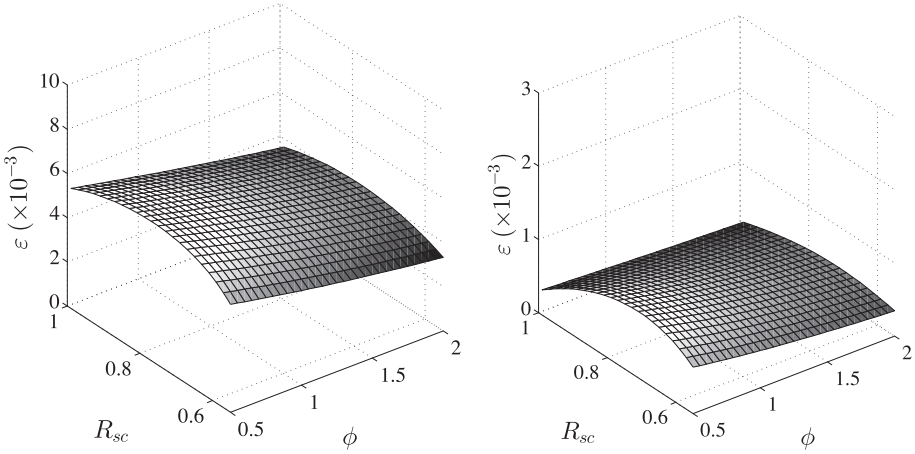

Fig. 2. Plastic strains induced by 0.01 stretching (left) and 0.003 stretching (right) as a function of the anisotropy index ϕ and solids content R_{sc}.

Table 2. The measurements and fitting procedures were presented in Erkkilä et al. (submitted for publication). In addition to the freely-dried sheets, the linear relationship between the drying shrinkage strain and hygroexpansion coefficient (Eq. (5)) can also be applied to restraint-dried sheets, but its validity does not extend to the sheets dried under additional stretch (Nordman, 1958). If $\beta_d = 0$, the ε_{ds} is estimated to have a positive strain (stretch) equal to b/a. The stretch component is subtracted from the term b/a by approximating the dry sample strain ε_d with the following equation

$$\varepsilon_d = -\frac{1}{a}\beta_d + \frac{b}{a}\left(1 - \exp\left(-100\frac{\beta_d}{a}\right)\right). \quad (6)$$

Table 2
The fitting parameters of Eq. (4)–(6) in the cases freely dried (fd) and restraint-dried (rd) samples made of SW, TMP or MIX pulp.

	k (–)	v (–)	a (–)	b (–)
SW fd	0.1557	−0.9809	2.6599	0.0244
SW rd	0.0535	−0.4987	2.6599	0.0244
TMP fd	0.1037	−1.3436	2.9596	0.0249
TMP rd	0.0687	−0.9002	2.9596	0.0249
MIX fd	0.1098	−1.3015	2.5054	0.0250
MIX rd	0.0439	−0.9015	2.5054	0.0250

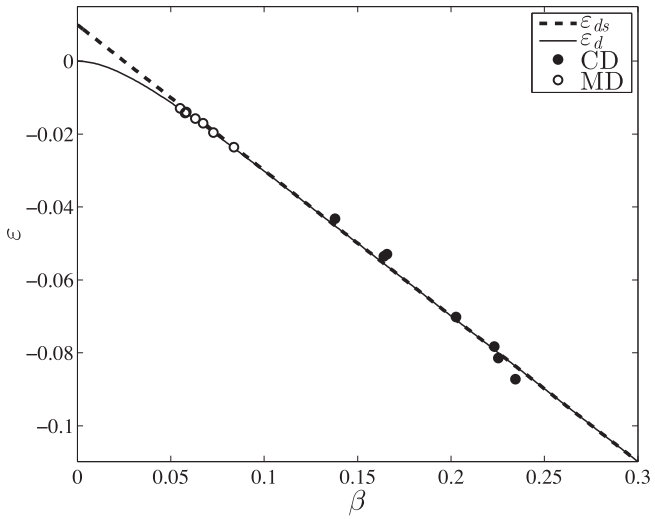

Fig. 3. The relationship between drying shrinkage strain ε and hygroexpansion coefficient β of the dry sample. Measured results of MIX samples are shown for cross direction in (CD) (with full dots), the machine direction (MD) (with open dots), the linear fitting Eq. (5) (with a dashed line) and relationship according to Eq. (6) (with a solid line).

Now if the hygroexpansion coefficient of the dry sample is $\beta_d = 0$, then the shrinkage of sample from wet to dry is $\varepsilon_d = 0$. The effect of the modification on the MIX pulp can be seen in Fig. 3. The measured data points from Erkkilä et al. (submitted for publication) are also presented.

Wahlström et al. (1999) and Wahlström (2004) introduced a function for the development of drying shrinkage strain ε_{h0} from wet to moisture ratio M:

$$\varepsilon_{h0} = \varepsilon_d \exp(B \times M) \tag{7}$$

where M is the moisture ratio and B is the fitting constant. For the freely-dried sheet, the value -2.6 was fitted for B by Wahlström (2004). As a function of solids content R_{sc}, Eq. (7) may be written in the form

$$\varepsilon_{h0} = \varepsilon_d \exp\left(B\left(\frac{1}{R_{sc}} - 1\right)\right). \tag{8}$$

Assuming that the hygroscopic strain behaves reversibly in infinitesimal solids content changes, the hygroexpansion coefficient can be approximated as a negative derivative of ε_{h0} with respect to solids content R_{sc}:

$$\beta = -\frac{\partial \varepsilon_{h0}}{\partial R_{sc}} = \frac{B}{R_{sc}^2}\varepsilon_d \exp\left(B\left(\frac{1}{R_{sc}} - 1\right)\right). \tag{9}$$

If the requirement $\beta(R_{sc} = 1) = \beta_d$ is set, the parameter B can be solved as

$$B = \frac{\beta_d}{\varepsilon_d}. \tag{10}$$

Lastly, the following equation for the hygroexpansion coefficient as a function of solids content can be derived:

$$\beta = \frac{\beta_d}{R_{sc}^2} \exp\left(\frac{\beta_d}{\varepsilon_d}\left(\frac{1}{R_{sc}} - 1\right)\right), \tag{11}$$

where β_d is defined by Eq. (4), and ε_d by Eq. (6). The hygroscopic shrinkage strain in the dry solids content interval $[R_{sc1} R_{sc2}]$ can be expressed as an integral

$$\varepsilon_h = -\int_{R_{sc1}}^{R_{sc2}} \beta dR_{sc}. \tag{12}$$

In the case of the isotropic sheet, the hygroexpansivity β as a function of R_{sc} and ε_h for interval $[0, R_{sc}]$ are presented in Fig. 4 for freely and restraint dried SW, TMP and MIX pulp samples. The dependency of β on ϕ and R_{sc} for freely and restraint dried MIX samples is presented in Fig. 5.

2.3. Continuum mechanical model

In the continuum mechanical model plane stress is assumed and the dependence between stress $\sigma = (\sigma_1, \sigma_2, \sigma_{12})^\top$ and strain $\varepsilon = (\epsilon_1, \epsilon_2, \epsilon_{12})^\top$ is defined by the generalized Hooke's law as

$$\sigma = C(\varepsilon - \varepsilon_h) \tag{13}$$

where C is the constitutive matrix and ε_h is the hygroscopic strain defined as

$$\varepsilon_h = -\begin{pmatrix} \beta_1 \\ \beta_2 \\ 0 \end{pmatrix} \Delta R_{sc} \tag{14}$$

where ΔR_{sc} is the solids content change and β_1 and β_2 are the hygroexpansion coefficients in the main direction and cross direction, respectively. Hygroexpansivities β_1 and β_2 and their dependence on ϕ and R_{sc} are defined by Eq. (11). Hill's yield function (Hill, 1948) is used to describe the yield surface. Hill's yield function is commonly used for paper and paperboard although there are known limitations related to it, for example, the origin symmetry of Hill's yield surface does not generally hold for paper or paperboard. An essential factor supporting the usage of Hill's yield function is the relatively simplicity of the parameter definition; in the case of paper the measurements needed for the determination of more exact yield

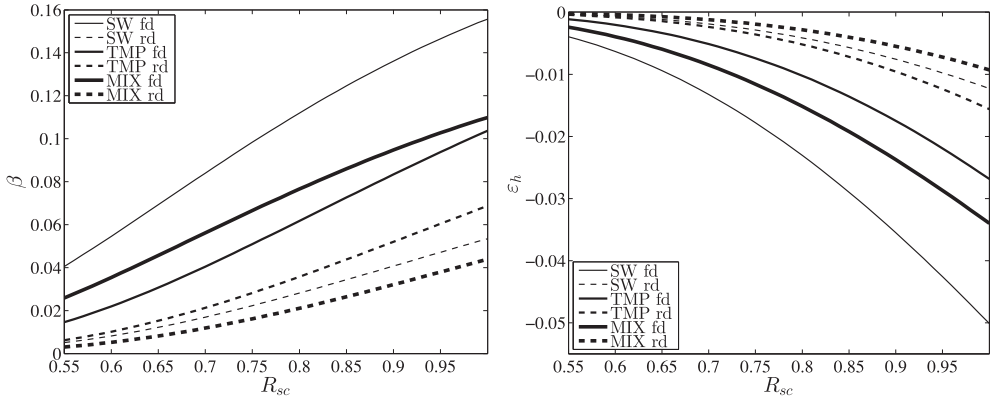

Fig. 4. Hygroexpansion coefficient β (left) and cumulative drying shrinkage strain ε_h (right) of an isotropic sheet as a function of solids content R_{sc}.

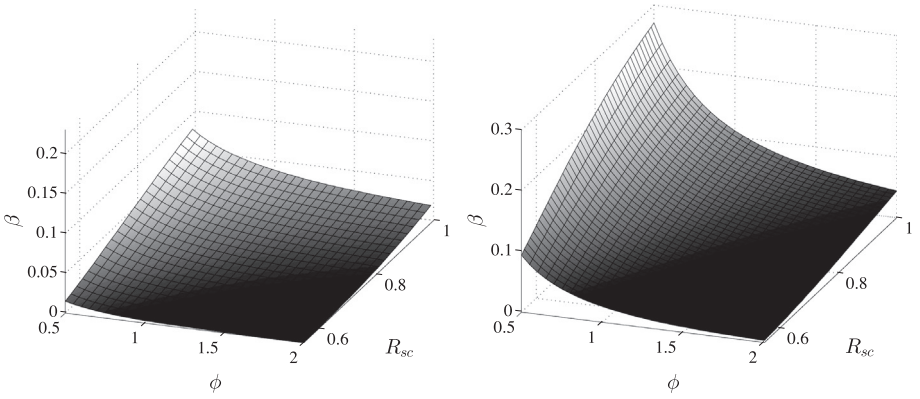

Fig. 5. The dependence of hygroexpansion coefficient β on anisotropy index ϕ and solids content R_{sc} for restraint dried (left) and freely dried (right) MIX samples.

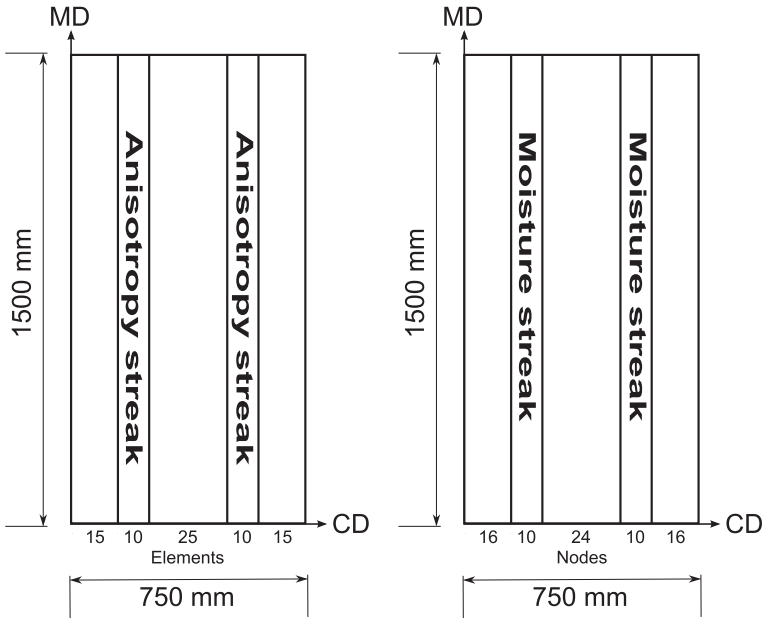

Fig. 6. The sample setup for the numerical simulations. The locations of the anisotropy (left) and moisture (right) streaks.

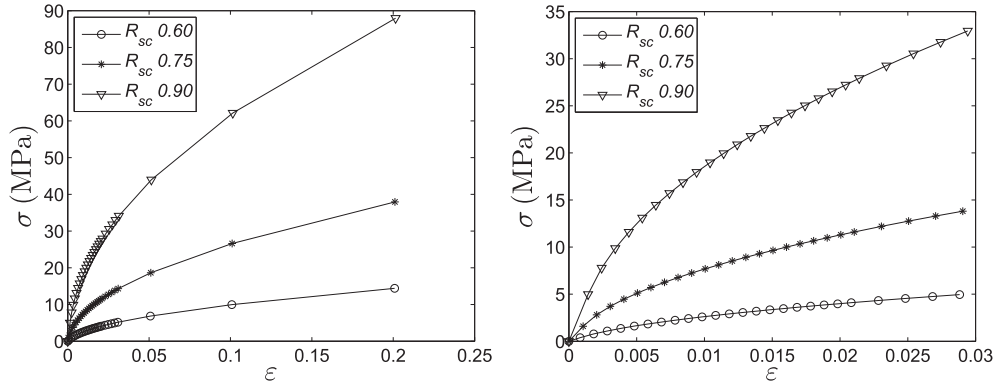

Fig. 7. Examples of discretized stress–strain relationships. The three solids content R_{sc} levels are 0.60, 0.75 and 0.90, and the anisotropy ξ = 2.0. Whole stress–strain curves (left), and the beginning of the curves of the left-hand figure (right).

surface are very complicated. According to Hoffman's approximation as found in Lipponen et al. (2008) the yield function has the form

$$f(\sigma) = \sqrt{\sigma_1^2 - \sigma_1\sigma_2 + \left(\frac{\sigma_{y,1}}{\sigma_{y,2}}\right)^2(\sigma_2^2 - \sigma_{12}^2) + \left(\frac{2\sigma_{y,1}}{\sigma_{y,45^\circ}}\right)^2\sigma_{12}^2} \qquad (15)$$

where σ_1, σ_2 and σ_{12} are the components of the stress tensor and $\sigma_{y,1}$, $\sigma_{y,2}$ and $\sigma_{y,45^\circ}$ are the yield stresses in the main direction, cross direction and the direction deviating 45° from the main direction, respectively. The elastic modulus is defined for directions 1, 2 and 45° as

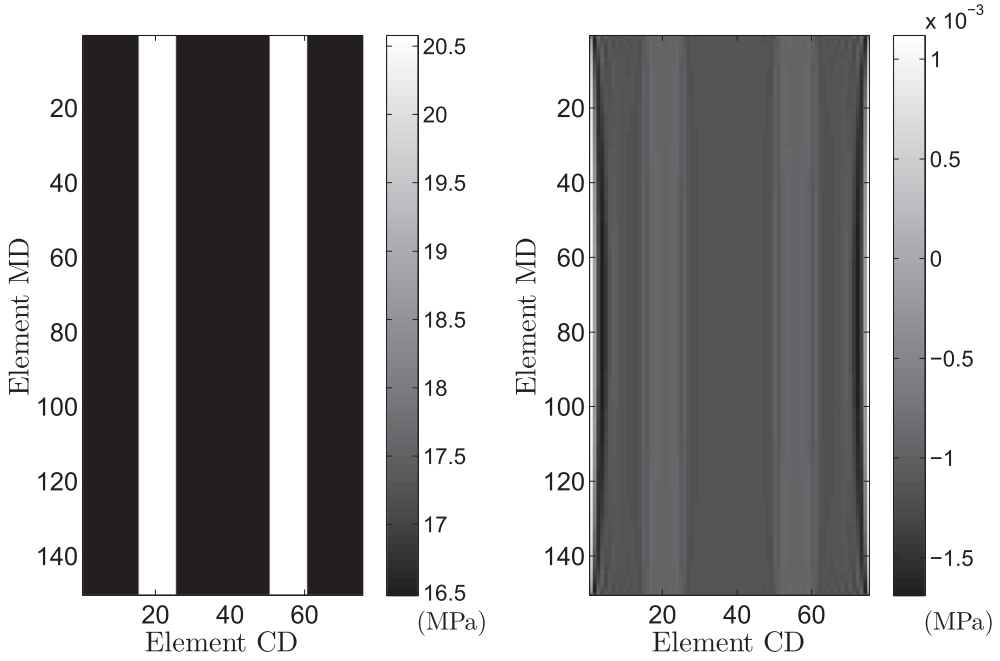

Fig. 8. MD stress (left) and CD stress (right) under 0.01 strain. Solids content R_{sc} = 0.9.

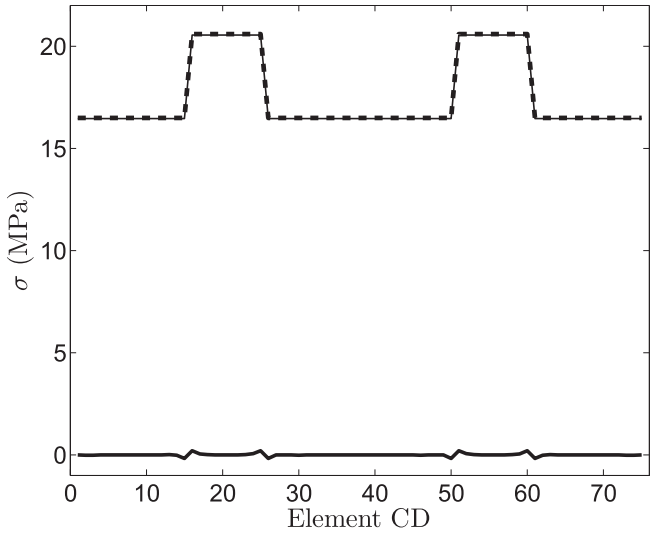

Fig. 9. CD profile of MD stress. The solids content R_{sc} = 0.9. Stress under 0.01 strain: the numerical result (solid narrow line), the one-dimensional analytical result (dashed line). The numerical result after release of the stretching (solid thick line).

$$E_i = \frac{\sigma_{y,i}}{\varepsilon_{y,i}}, \tag{16}$$

where $\varepsilon_{y,i}$ is the yield strain in the direction specified by the subscript *i*. All in-plane stress and strain parameters are defined by Eq. (2). The shear modulus is approximated as in Gibson (1994):

$$G_{12} = \frac{1}{\left(\frac{4}{E_{45^\circ}} - \frac{1}{E_1} - \frac{1}{E_2} - \frac{2\nu_{12}}{E_1}\right)}, \tag{17}$$

where ν_{12} is Poisson's ratio defined as

$$\nu_{12} = (0.015(1 - R_{sc}) + 0.15)\phi_1, \tag{18}$$

where ϕ_1 is the anisotropy index of the main direction. The dependence of ν_{12} on the anisotropy index and solids content is roughly based on the results presented in Yeh et al. (1991). By Maxwell's relation Poisson's ratio ν_{21} is defined as $\nu_{21} = \nu_{12}E_2/E_1$.

2.4. Sample setup and numerical solution

For the simulation examples, the finite element method (FEM) was used to obtain the numerical solution. Simulations were performed using ABAQUS/standard and shell element S4R with

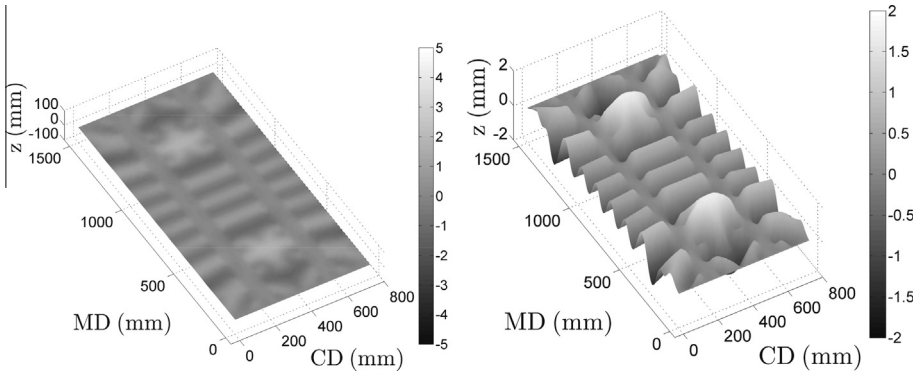

Fig. 10. Simulated out-of-plane deformations after the sample was stretched to 0.01 strain in the MD and released. In the streaks, the fiber orientation anisotropy ξ = 2.2 and in the surrounding areas ξ = 1.8. Solids content R_{sc} = 0.9.

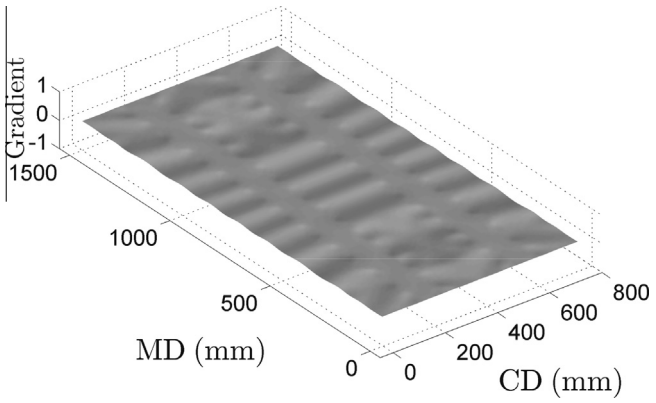

Fig. 11. Gradient representation of the out-of-plane deformation map in Fig. 10.

composite structure; see ABAQUS (2013). The sample size was 1500 mm in the machine direction (MD) and 750 mm in the cross machine direction (CD); see Fig. 6. The thickness of the sample was 0.1 mm. The element size in both MD and CD was 10 mm, and in the thickness direction, the element was divided into eight layers of equal thickness. Since there were eight material layers, the solids content was defined by nine equally spaced interfaces in the thickness direction. In all simulations, except for the case where the thickness directional solids content variation was studied, the solids content was the same in eight of the interfaces. The solids content of the top surface was 0.5% lower than in other interfaces. This approach was used to eliminate the symmetry of the sample, enabling the potential out-of-plane deformation.

In the numerical solution approach, the anisotropy, solids content, and stress–strain curve is discretized. When solids content and stress–strain space are considered, a linear behavior between defined points is assumed. In the case of anisotropy, the anisotropy is rounded to the nearest discrete value. The anisotropy was discretized with 0.1 intervals covering anisotropies between 1.0 and 6.0. The solids content dependence of the elastic properties, isotropic hardening, Hill's yield surface and moisture expansion coefficient was discretized with a resolution of 1%, covering the solids content values from 55% to 100%. The stress–strain curve was discretized into 29 unequal intervals; see Fig. 7. The first point from the origo is the yield point defining the borderline between elastic and plastic behavior. Higher resolution was used with small plastic strains, as can be seen from Fig. 7.

The sample may have one of three different anisotropy-solids content-structures (Fig. 6), contingent on the simulation case scenario:

1. The solids content is constant throughout the sample, while the anisotropy has two 100 mm through-thickness MD streaks. Within the streaks, the anisotropy ξ is 2.2, while in the surroundings, anisotropy ξ is 1.8.
2. The anisotropy is constant throughout the sample ($\xi = 2$), while the solids content has two through-thickness MD streaks.
3. The anisotropy is constant throughout the sample ($\xi = 2$), while the solids content varies in the thickness direction.

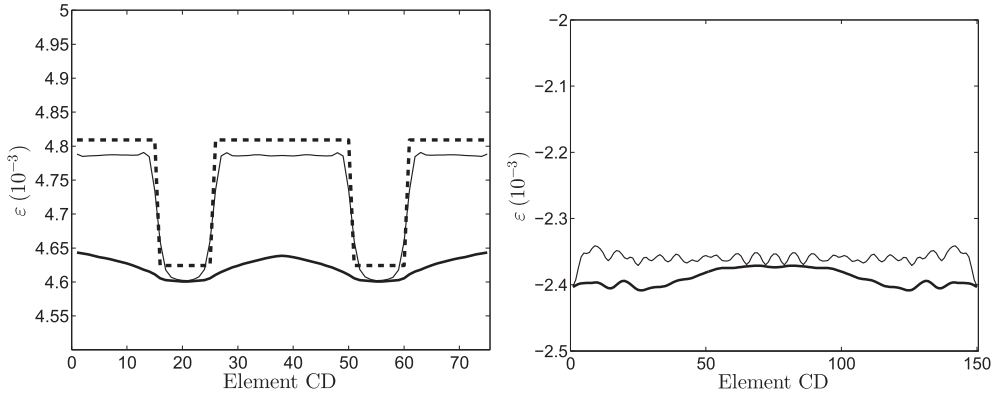

Fig. 12. The CD profile of the MD plastic strains (left), and the MD profile of the CD plastic strain (right) after the sample was stretched to 0.01 strain in the MD and released. The in-plane deformation of the simulated sample (solid thick line), the strain determined using integrated length of the simulated sample (solid narrow line) and the plastic strain using analytical one-dimensional model (dashed line). Solids content R_{sc} = 0.9.

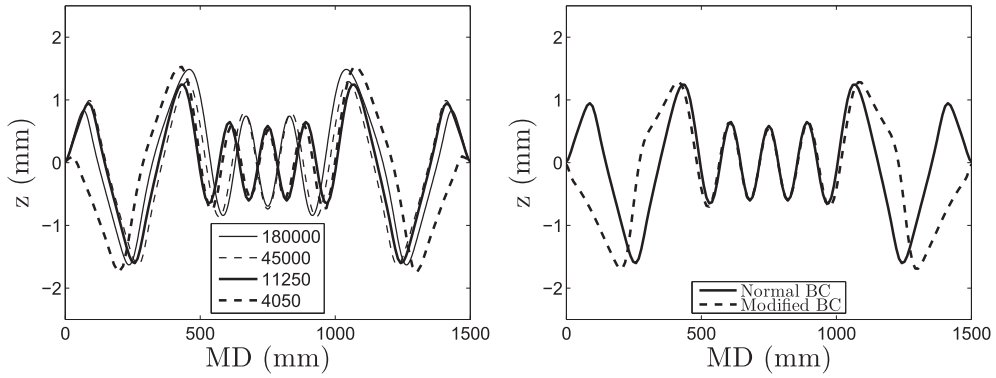

Fig. 13. MD out-of-plane profile from the middle of the sample when different number of equal sized elements are used in the numerical solution procedure (left). In the right figure, result obtained from this normal simulation setup (11250 elements) is compared with case where out-of-plane displacement and rotations are restricted in the vertical edges (CD = 0 mm and CD = 750 mm), see Fig. 6.

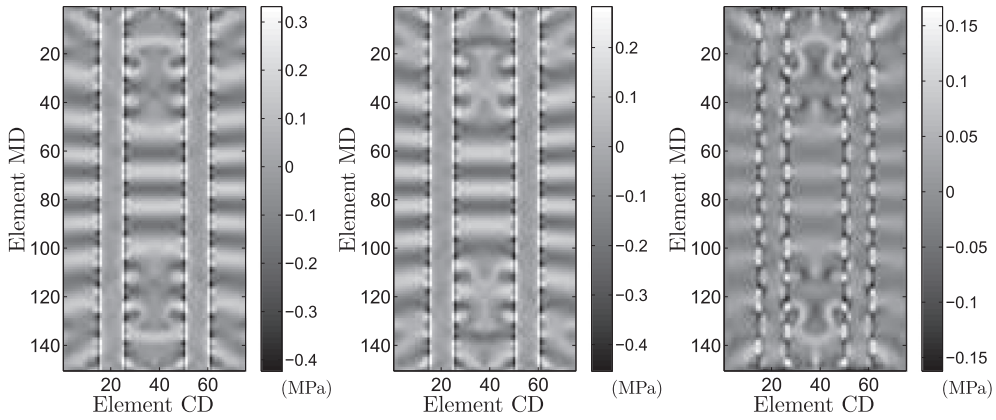

Fig. 14. Local MD and CD stresses after the sample was stretched to 0.01 strain in the MD and released. The bottom side MD stress (left), the top side MD stress (middle) and the bottom side CD stress (right). Dry solids content R_{sc} = 0.9.

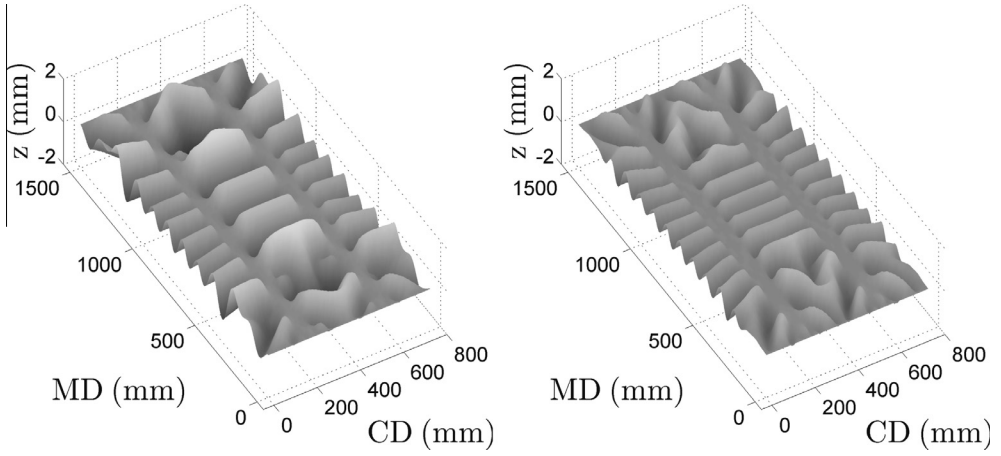

Fig. 15. Simulated out-of-plane deformations after the sample was stretched to 0.01 strain in the MD and released. The solids content R_{sc} = 0.75 (left) and solids content R_{sc} = 0.60 (right). In the streaks, the fiber orientation anisotropy $\xi = 2.2$; in the surrounding area ξ = 1.8.

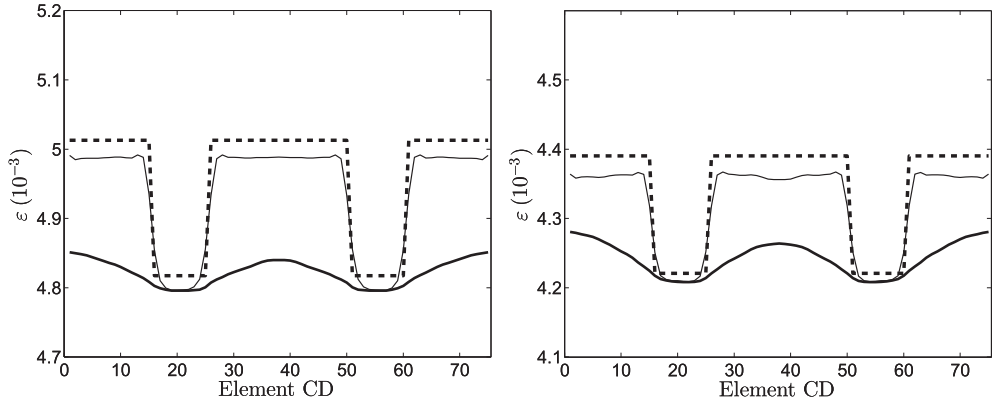

Fig. 16. CD profile of the MD plastic strains after the sample was stretched to 0.01 strain in the MD and released. The solids content R_{sc} = 0.75 (left), and the solids content R_{sc} = 0.60 (right). The in-plane deformation of the simulated sample (solid thick line), the strain determined using integrated length of the simulated sample (solid narrow line) and the plastic strain using analytical one-dimensional model (dashed line).

One or several boundary conditions were used during the simulation, depending on the case in question. However, throughout every simulation the following boundary conditions are used:

1. The MD and CD displacement of the middle node (MD = 750 mm, CD = 370 mm, see Fig. 6) of the sample was restricted.

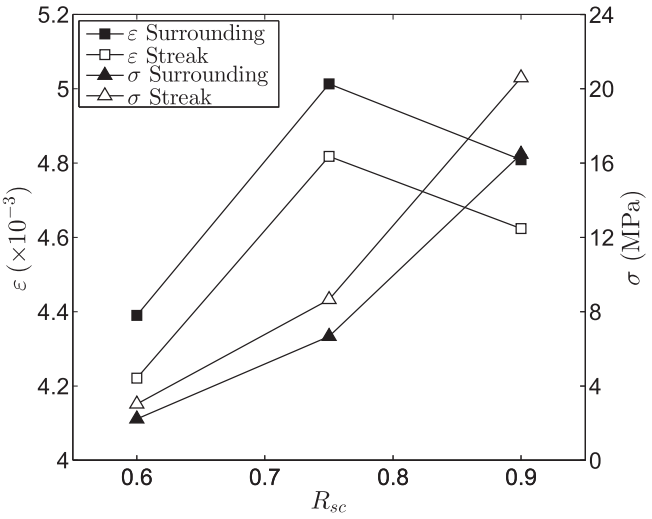

Fig. 17. Stress, σ, under 0.01 strain and the plastic strain, ε, after release.

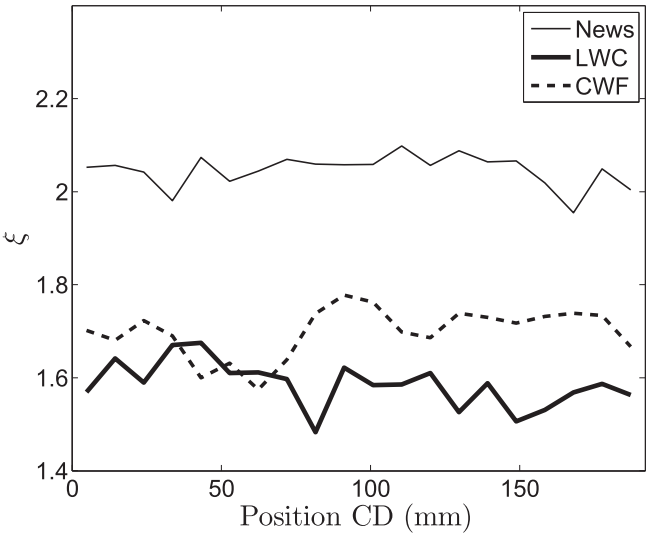

Fig. 18. Measured fiber orientation anisotropy CD profiles for News, LWC and CWF samples.

2. The out-of-plane displacement and rotations of the nodes located at the horizontal edges (MD = 0 mm and MD = 1500 mm, see Fig. 6) were restricted.

3. The numerical simulations and one-dimensional analytical results

3.1. Elasto-plastic deformation

In this section, some examples using elasto-plastic model in stretching conditions without solids content changes are presented. In the first case, the sample with the anisotropy streaks depicted in Fig. 6 had a solids content of 90%. In the simulation, 1% MD stretching was applied to the sheet, while the CD was unconstrained. The MD and CD stress prevailing during the stretching is presented in Fig. 8. The simulated MD stresses in the streaks and other positions were equivalent to MD stresses determined analytically from the one-dimensional material model, as can be seen from the CD profiles of the MD stress from Fig. 9. Through uniform stretching higher tension was created in the streaks where the anisotropy is higher. After release of the stretching, the stress dropped back to zero, and only some minor disturbance could be detected in the boundary areas of the streaks (Fig. 9). The out-of-plane deformations appeared after the stretch was released; see Fig. 10. The out-of-plane deformations were small compared to the in-plane dimensions of the simulated sample. For topography examination, the z-axis will henceforth be zoomed in on, as in Fig. 10 (right). For visual inspection, the MD gradient image is presented in Fig. 11. The gradient image simulates the inclined illuminated situation and may reveal some small-scale sharp details that are normally quelled by the higher amplitude of long wavelengths in the topography map detection. In reality, the visual appearance of an out-of-plane deformation depends highly on illumination and the detection angle, the glossiness of the surface and the ratio of the wavelength to detection distance.

The in-plane deformation and strain in MD and CD are presented in Fig. 12. The strain of the deformed sample was determined by discrete integration. The plastic MD strain determined analytically using a one-dimensional material model (Eq. (2)) is drawn as dashed line in Fig. 12. The narrowing of CD (see Fig. 12) was determined by Poisson's ratio. The plastic strain differences between the streaks and other areas caused the tight streaks and buckling in the slack surrounding areas of sheet, as is presented in Fig. 10. Buckling is highly dependent on boundary conditions, element size, disturbance, etc., so the topography result can only be considered as approximate or suggestive, see Fig. 13. Local stresses of the bottom and top sides could be detected, as could be expected, as being negative to each other: the local curl caused shrinkage in the concave surface and positive strain in the convex surface of the local buckle (see Fig. 14). The total stress, however, reached zero, leaving no global internal stresses, except some disturbances near the interfaces between regions with different anisotropies (as shown in Fig. 9).

For the 75% and 60% solids contents, simulations with 1% stretching were performed. In the case of 60% solids content, the decreased stiffness caused a higher frequency in waviness when compared to 75% or 90% solids contents; see Fig. 15. As can be expected, the stress applied by the 1% stretching did increase toward higher dry solids content (Fig. 17). The highest plastic strain at the middle solids content (75%) results from elasto-plastic material model, see Fig. 2. This is also consistent with Land's study (Land et al., 2008). However, higher plastic strain level did not increase the plastic strain difference of the streaks and surrounding areas significantly (see Figs. 16 and 17). In any case, all plastic strain differences were small, below 0.02%, but buckling behavior was estimated by the simulations.

1% stretching or even more stretching of a wet sheet is common when the web is transferred from the press section to the drying section of a paper machine. In other stages, when the dry solids content of sheet is higher, a 1% stretch is unusual, since the tension needed for web runnability rises due to the drying shrinkage. To clarify the phenomena occurring in these examples, the anisotropy difference between streaks and other areas was higher than is usually found in machine made papers. Anisotropy profiles of three production machine samples – newsprint (News), light weight coated (LWC) and coated wood free (CWF) – are presented in Fig. 18. These profiles were measured by layered fiber orientation measurement (Lipponen et al., 2009) and the anisotropy values were averaged over the layers. The samples were 192 mm × 192 mm, and the fiber orientation was determined from 20 adjacent areas each having a length of 192 mm in the MD and a width of 192/20 mm in the CD. In these three samples the deviation (max–min) of the profile was approximately 0.2, while in simulations, the used difference of anisotropies between streaks and

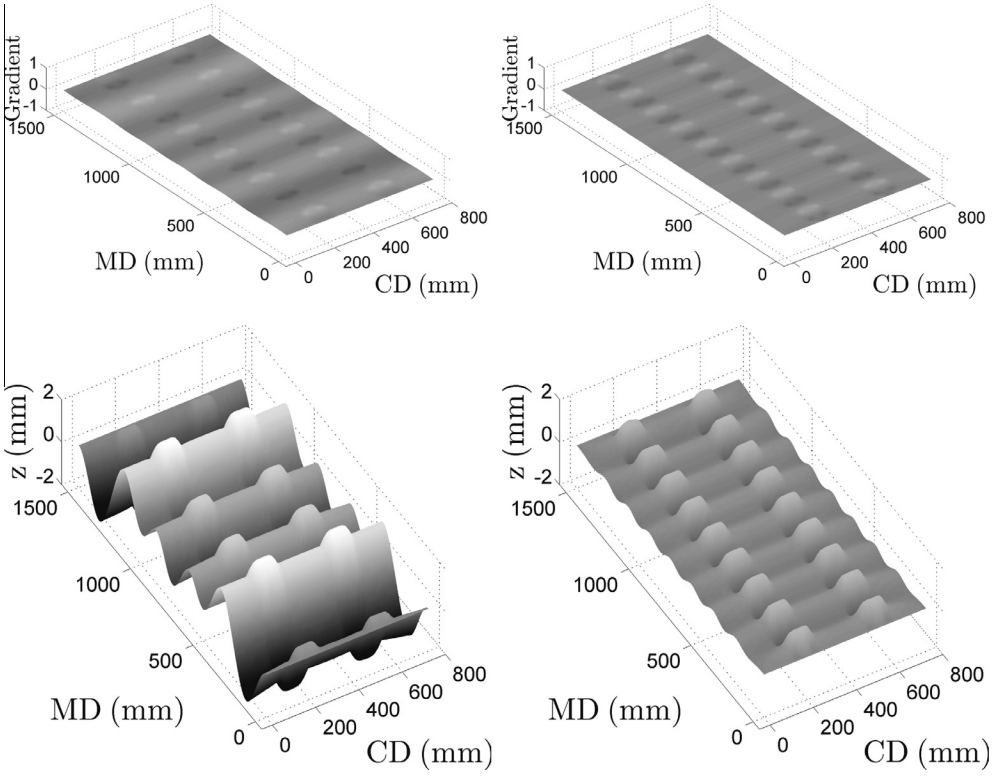

Fig. 19. Simulated out-of-plane deformations when the surroundings of the streaks are dried from solids content R_{sc} = 0.90 to R_{sc} = 0.91. In the upper row the gradient images and in lower row topography pictures. In the left column the sample has been unconstrained during drying while in right column the MD shrinkage is restricted during drying. Homogenous structure with anisotropy $\xi = 2$.

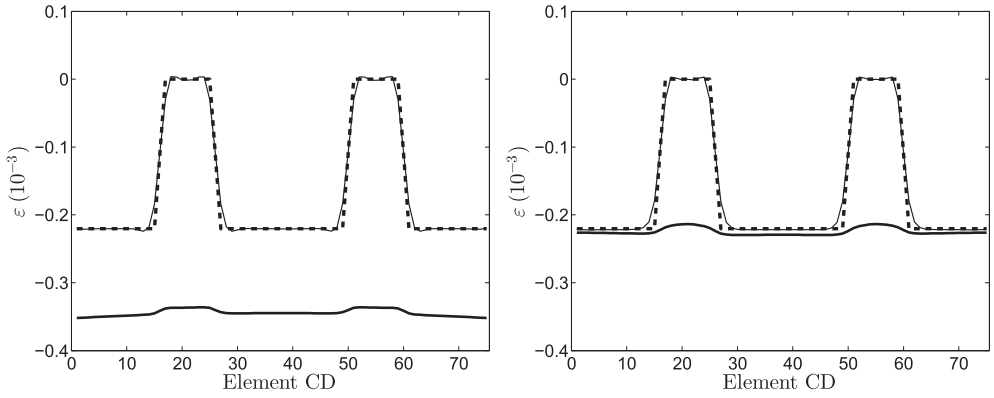

Fig. 20. CD profiles of MD shrinkage strains when the surroundings of the streaks are dried from dry solids content R_{sc} = 0.90 to R_{sc} = 0.91. The in-plane deformation of the simulated sample (solid thick line), the strain determined using integrated length of the simulated sample (solid narrow line) and the hygroscopic strain using analytical one-dimensional model (dashed line). Unconstrained drying (left) and MD shrinkage is restricted during drying (right).

surrounding areas was 0.4. However, it should be noted that anisotropy variations are often clearly higher if different layers or local deviations are studied (Erkkilä et al., 1998; Lipponen et al., 2009).

3.2. Hygroscopic deformations

In this section, simple examples of the effect of moisture changes on dimensional deformations using the hygroexpansivity-shrinkage model are presented. Obviously, even when the purpose is solely to study the effects of hygroexpansivity through finite element simulations, the results are not independent of the material model. However, using Eq. (12), the one-dimensional analytical results may indeed be solved directly without a material model. In the first example of this section, the moisture streaks of a structurally homogeneous anisotropic sheet (ξ = 2) were arranged as illustrated in Fig. 6. The sample was dried rendering a solids content change of 90% to 91%, except in the areas of the 100 mm wide streaks, in which no changes were applied; i.e. the solids content in those streaks remained at 90%. The drying was performed either under MD restraint with unconstrained CD, or under no constraint for both MD and CD, so that the sample was free to deform during the drying in all directions. The MD restraint sample was released after drying and allowed to deform freely. The fitting parameters of the restraint-dried MIX sheet were used in these simulations (see Table 2 and Eqs. (4) and (6)). The gradient and topography images are presented in Fig. 19. Freely and restraint-dried cases

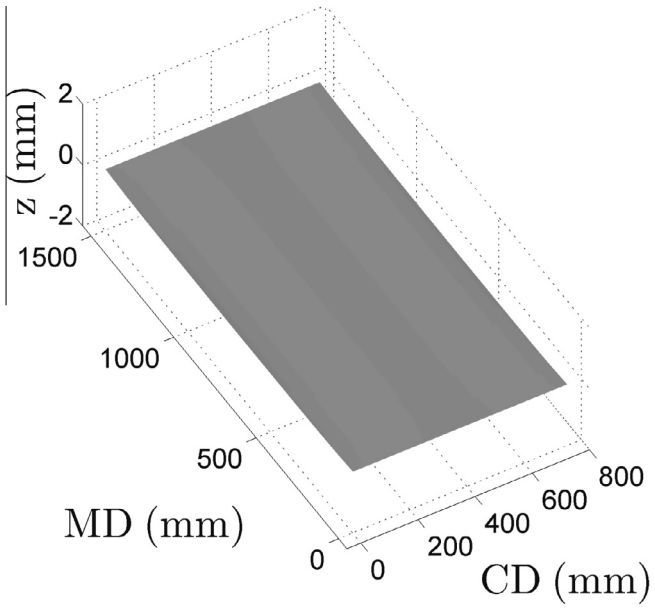

Fig. 21. Simulated out-of-plane deformations when in the first step the surrounding areas of the streaks were dried from the solids content R_{sc} = 0.90 to R_{sc} = 0.91, and in the second step equal drying was performed for the streaks. Homogenous structure with anisotropy $\xi = 2$.

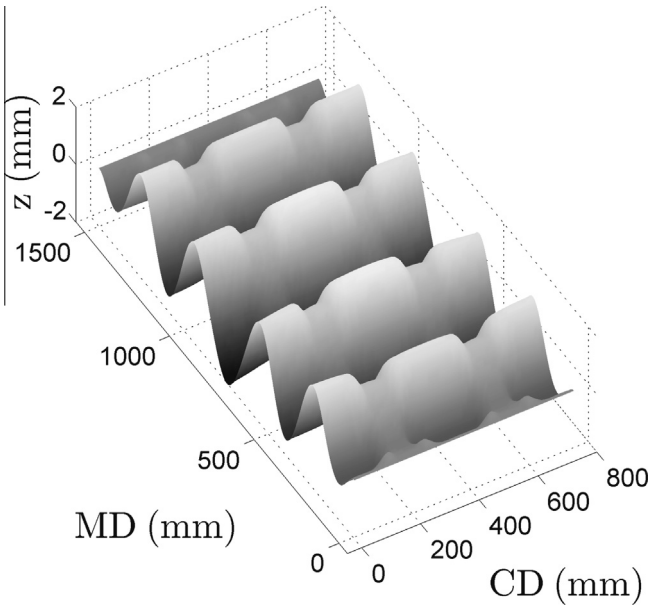

Fig. 23. Simulated out-of-plane deformation. In the first step, the sample was stretched to 0.01 strain in the MD and released, and in the second step, it was freely dried from solids content R_{sc} = 0.60 to R_{sc} = 0.65. In the streaks, the fiber orientation anisotropy $\xi = 2.2$; in the surrounding areas ξ = 1.8.

were almost identical when the average CD profiles of the MD shrinkage strain were compared and furthermore were congruent with the analytical one-dimensional results; see Fig. 20. Visually, the biggest difference could be detected in the buckling behavior. The overall low frequency bending of the freely dried sheet lowered the frequency of waviness in the streaks and smoothed the tensions slightly in the streak boundaries (the maximum-minimum difference was 232 kPa for the freely dried sample and 244 kPa for the MD restraint-dried sample). If in the following step the streak areas are dried equivalently from 90% to 91% (Fig. 21), all out-of-plane deformations disappear, the internal stresses are reduced to zero at every position, and the amount of shrinkage is equal everywhere and congruent with the one-dimensional hygroexpansivity model. No plastic deformations arose either in restraint-dried or freely dried cases under such a small stress difference (808 kPa (tension = 80.8 N/m) in the restraint sample) or due to shrinkage differences, only 0.022% between the surrounding and streak areas.

Also, anisotropy affects hygroexpansivity. A sheet with anisotropy streaks was dried from 60% to 65% solids content without any constraints in the MD nor CD. The out-of-plane deformation and CD profile of the MD shrinkage strains are presented in Fig. 22. The streaks having higher anisotropy levels shrunk less than the other areas. The strain difference is very small, only 0.0041%. In order to more purely study the behavior of the hygroscopic model without the interference of plasticity, the studied moisture changes were kept low, and all simulation results corresponded well with the results of the one-dimensional hygroexpansivity model.

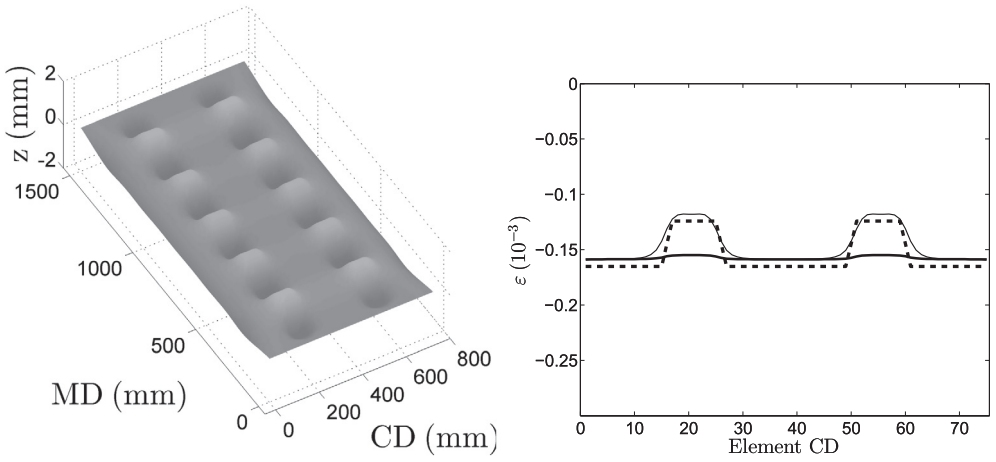

Fig. 22. The out-of-plane deformation (left), and the CD profile of MD hygroscopic strains (right) after the sample containing anisotropy streaks was dried from solids content R_{sc} = 0.60 to R_{sc} = 0.65. In the right-hand figure, the in-plane deformation of the simulated sample (solid thick line), the strain determined using integrated length of the simulated sample (solid narrow line) and the hygroscopic strain using analytical one-dimensional model (dashed line).

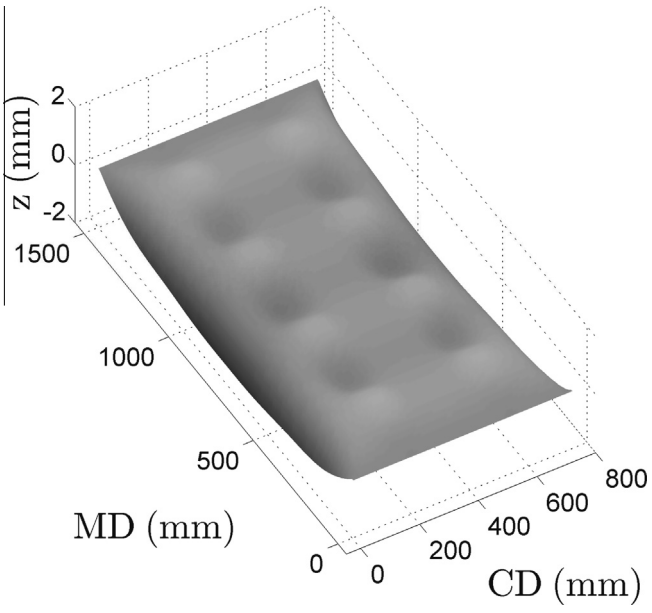

Fig. 24. Simulated out-of-plane deformation. In the first step, the sample was stretched to 0.01 strain in the MD and released, and in the second step, it was freely dried from solids content R_{sc} = 0.60 to R_{sc} = 0.75.

3.3. Brief study of interactions between moisture changes and stretching

The aim in the previous sections was to demonstrate the behavior of the material model and the hygroexpansivity model separately, although the finite element simulations of hygroexpansivity are not independent of the material model in any case. To study simultaneous and interactive phenomena, including factors of drying and draw from both the hygroexpansivity model and the material model, a few examples are presented here.

Starting with a baseline anisotropy streak case (as presented in Section 3.1) having a solids content of 60%, the different drying conditions could be applied. The first step was thus a draw of 1% in the MD. In the second step, the draw was released, and then the sheet was dried freely from a solids content of 60% to 65%. The second step was fundamentally the same as the anisotropy streak case of Section 3.2, excepting for initial plastic strain differences and minor internal stresses at the streak boundaries. The deformation occurring after this second step is presented in Fig. 23. After adding up the CD profiles of MD strain solved by the one-dimensional approach of the first step (Fig. 16, right) and the second step (Fig. 22), an equivalent profile was achieved as that of the finite element simulation; see Fig. 26. When the drying in the second step were continued to a solids content of 75%, almost all deformations arising from the streaks disappeared (Fig. 24), since the shrinkage amount is lower in the streak areas. A significant change in deformations can be detected if the 1% draw is not released before the second step drying. The drying shrinkage increases the MD tension further, resulting in an increase in the plastic strain level as well as in the difference between the streaks and surrounding areas in the MD (Figs. 25, 26 and Table 3).

Table 3
The strains in the streaks and surrounding areas from Fig. 26.

	Streak (%)	Surrounding (%)	Difference (%)
65 fd	0.4075	0.4213	0.0138
75 fd	0.3543	0.3551	0.0008
65 rd	0.4475	0.4647	0.0173
75 rd	0.4609	0.4771	0.0161
One-dimensional	0.4097	0.4225	0.0128

In the second example, the anisotropic homogeneous sample ($\xi = 2$) was freely dried from a solids content of 80% to 90% or 95%, so that in the first step solids content profiles in the thickness direction were applied through the sample as is presented in Fig. 27. The profiles used are roughly based on Östlund's simulations for symmetric convective drying. The sample with basis weight 300 g/m^2 was dried symmetrically from R_{sc} = 0.435 to R_{sc} = 0.997, for details see Östlund (2006). Only the high solids content profile (mean $R_{sc} \approx 0.85$) was used. In the second step, the whole paper would finally achieve a uniform solids content of 90% or 95%. According to the simulations of this study (Fig. 27) every tested solids content profile generates plastic strain differences between layers. The simulated stresses (Fig. 27) are same order of magnitude as measured results in Östlund et al. (2004) despite of the different material parameters etc. between the studies. The plastic strains of the layers in the MD and in the CD are presented in Table 4. The higher plastic strain in the CD than in the MD resulted from the higher shrinkage tendency and from the different plasticity properties in the CD than in the MD in the anisotropic sheet.

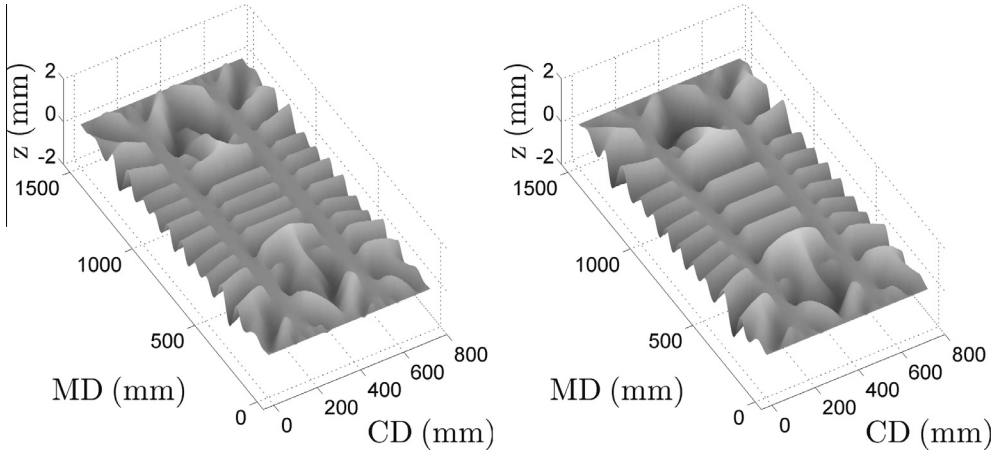

Fig. 25. Simulated out-of-plane deformation. In the first step, the sample was stretched to 0.01 strain in the MD, and in the second step, it was dried under MD restraint from solids content R_{sc} = 0.60 to R_{sc} = 0.65 (left), and from solids content R_{sc} = 0.60 to R_{sc} = 0.75 (right).

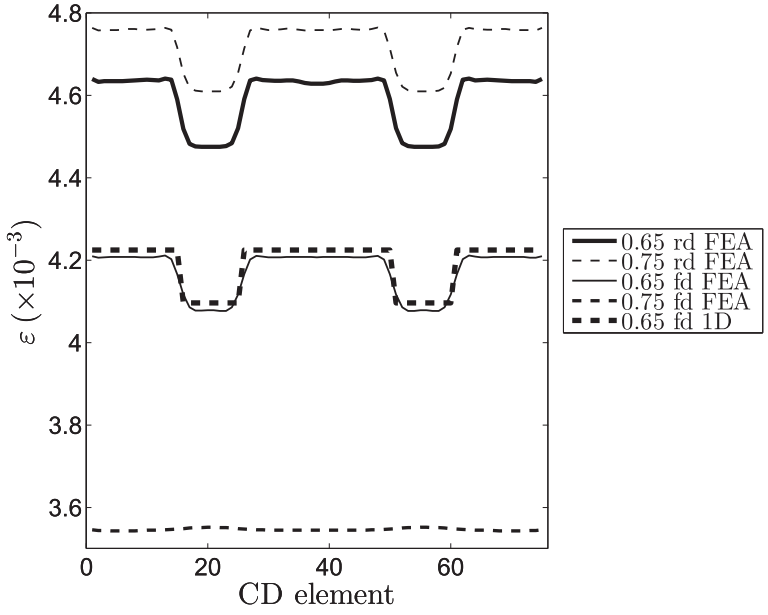

Fig. 26. CD profiles of MD deformations for the cases depicted in Figs. 23–25. The analytical one-dimensional result corresponding to the case of Fig. 23 is presented by a thick dashed line.

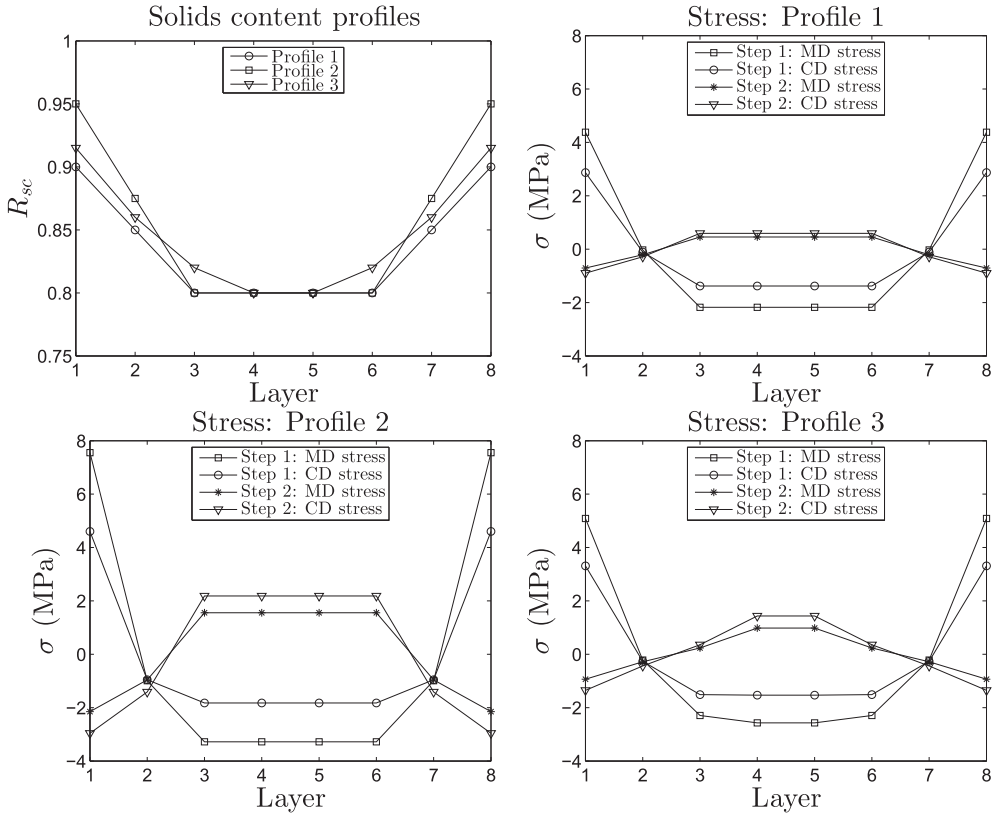

Fig. 27. The MD and CD stress of different layers, when in the first step different through-thickness solids content profiles (top-left) are applied. In the initial situation solids content trough the sample is R_{sc} = 0.80 and in the second step every layer is dried either to R_{sc} = 0.90 (solids content profile 1) or R_{sc} = 0.95 (solids content profiles 2 and 3).

Table 4
The plastic strains in the layers from Fig. 27.

	Profile 1		Profile 2		Profile 3	
Layer	MD (%)	CD (%)	MD (%)	CD (%)	MD (%)	CD (%)
1 and 8	0.0068	0.0418	0.0160	0.0838	0.0084	0.0497
2 and 7	0	0	0	0	0	0
3 and 6	−0.0084	−0.0607	−0.0313	−0.1966	−0.0061	−0.0437
4 and 5	−0.0084	−0.0607	−0.0313	−0.1966	−0.0152	−0.1028

4. Conclusions

The hygro-elasto-plastic model introduced herein offers the possibility to study several complex phenomena of such orthotropic planar materials as board or paper. The elasto-plastic model and hygroexpansivity-shrinkage model based on experimental results can be solved analytically and separately in one dimension, but the full potential of these models is achieved through the

numerical solution of a continuum mechanical model. With finite element analysis, the simultaneous and interactive situations combining these two separate models as well as the effect of plastic and hygroscopic strains on the buckling behavior of a sheet or web can be simulated. The time- or history-dependent behaviors are not implemented on the introduced hygro-elasto-plastic model. Thus, the applicability of the model on studies of storage and multi-chained processes is limited. The input parameters of the model are the fiber orientation anisotropy index (Erkkilä et al., 2013), the dry solids content, the external strain or stress and the change in the dry solids content. The use of the anisotropy index instead of that of traditional fiber orientation anisotropy simplified the handling of different in-plane directions. Usually, the hygroexpansion coefficient has been considered to characterize the deformation of a dry paper subject to a moisture change, independently of the moisture content level, although some stress relaxation and moisture history dependence may have been involved (Uesaka et al., 1992). In this study, the dry solids content dependent hygroexpansivity, over the entire range from wet to dry, has been suggested. A few different parameters to model hygroexpansivity depending on the pulp type of the sample and on the free or restrained drying conditions can be selected.

With the use of the finite element method, different sheet structures and dimensions can be applied, such as sheets or webs including anisotropy, basis weight or moisture content variation in-plane and throughout the different layers. The application possibilities are versatile for studies on paper web or sheet behavior in drying, converting, printing or copying processes. The corresponding defects may include, for example, shrinkage profiles, misregistration in printing, deformation of boxes, different buckling phenomena such as cockling, curling and heatset web offset fluting, internal stresses build up due to the two sidedness of different processes and the streakiness of the web.

To demonstrate the model responses, a few examples of the effect of anisotropy and moisture streaks of otherwise homogenous anisotropic sheets on strain differences and buckling have been presented. Also, the internal stresses caused by the drying process with different layers drying at different stages have been discussed. Very small plastic strain differences may cause buckling, but how visually disturbing these out-of-plane deformation defects are depends on paper or board grade and usage. This kind of buckling streakiness is considered as a defect, and is often called the bagginess of a paper web. The baggy paper web brings up the risk of wrinkling, which is reported to increase if the strain difference is higher than 0.1%, although for some thin papers, a strain difference of only 0.01% is enough to cause noticeable problems (Roisum, 1996). In the examples of this work, the strain differences have been more on the order of 0.01% than 0.1%. The simulation cases were kept simple and the stretching and dry solids content changes were selected to be small compared to the real total drying process of a paper machine. This enables to observe the hygroexpansion and plastic strains separately, to compare the analytical and numerical in-plane deformations and to understand the phenomena comprehensively.

The complexity of the interactive and simultaneous behavior of hygroexpansivity and plasticity was revealed even with the simple examples presented in this paper. For example, the streaks having a higher anisotropy level than in the surrounding areas appeared as tight streaks after stretching in the MD because of the lower plastic strain in the MD. The free drying performed subsequently to the stretching-releasing procedure may compensate for the difference in the plastic strains, because the MD shrinkage tendency of the high anisotropy streaks is lower than that of the surrounding areas. However, if drying is done under restraint, the lower shrinkage of the streaks may even further increase the plastic strain difference between the streaks and surrounding areas. Land's experimental study (Land et al., 2008) of the effect of the moisture streaks on permanent strain differences also showed that the releasing of tension at different stage of drying is a significant factor.

According to the simulation results of this study, the buckling could be caused by both the anisotropy and the moisture streaks. The more challenging task is to determine in which cases the generated buckling and strain differences remain as permanent plastic strain differences, perhaps over subsequent converting processes; and even further, in which cases they cause problems during paper making and converting processes. Some problems of moisture streaks arising from the drying section may well vanish in the coating or calendaring processes, where moisture or heat is brought to the paper web. Structural streaks, such as anisotropy or basis weight streaks, stay in the paper once formed, and may create problems at any stage of the paper life cycle.

Acknowledgements

Simulations were performed by commercial software ABAQUS which was licensed to CSC (the Finnish IT center for science).

References

ABAQUS, 2013. ABAQUS Documentation. Dassault Systèmes, Providence, RI, USA.
Alava, M., Niskanen, K., 2006. The physics of paper. Rep. Prog. Phys. 69, 669–723.
Alfthan, J., 2004. The effect of humidity cycle amplitude on accelerated tensile creep of paper. Mech. Time Depend. Mater. 8 (4), 289–302.
Bloom, F., Coffin, D.W., 2000. Modelling the hygroscopic buckling of layered paper sheets. Math. Comput. Model. 31 (8–9), 43–60.
Brezinski, J.P., 1956. The creep properties of paper. Tappi 39 (2), 116–128.
Castro, J., Ostoja-Starzewski, M., 2003. Elasto-plasticity of paper. Int. J. Plast. 19, 2083–2098.
Constantino, R.P.A., I'Anson, S.J., Sampson, W.W., 2005. The effect of machine conditions and furnish properties on paper CD shrinkage profile. In: Proceedings of 13th Pulp and Paper Fundamental Research Symposium, Cambridge, pp. 283–306.
de Ruvo, A., Lundberg, S., Martin-Löf, S., Södermark, C., 1976. Influence of temperature and humidity on the elastic and expansional properties of paper and the constituent fibre. In: The Fundamental Properties of Paper Related to Its Uses, Transactions of the Symposium, British Paper Board Industry Federation, London, pp. 785–806.
Erkkilä, A.-L., Pakarinen, P., Odell, M., 1998. Sheet forming studies using layered orientation analysis. Pulp Pap. Canada 99 (1), 81–85.
Erkkilä, A.-L., Leppänen, T., Hämäläinen, J., 2013. Empirical plasticity models applied for paper sheets having different anisotropy and dry solids content levels. Int. J. Solids Struct. 50, 2151–2179.
Erkkilä, A.-L., Leppänen, T., Ora M., Tuovinen, T., Puurtinen, A., submitted for publication. Hygroexpansivity of anisotropic sheets. Nordic Pulp Pap. Res. J.
Fahey, D.J., Chilson, W.A., 1963. Mechanical treatments for improving dimensional stability of paper. Tappi 46 (7), 393–399.
Fellers, C., Westerlind, B., de Ruvo, A., 1983. An investigation of the biaxial failure envelope of paper – experimental study and theoretical analysis. In: Proceedings of Fundamental Research Symposium, Cambridge, pp. 527–559.
Gates, E.R., Kenworthy, I.C., 1963. Effects of drying shrinkage and fibre orientation on some physical properties of paper. Pap. Technol. 4 (5), 485–493.
Gibson, R.F., 1994. Principles of Composite Material Mechanics. McGraw-Hill Inc.
Glynn, P., Jones, H.W.H., Gallay, W., 1961. Drying stresses and curl in paper. Pulp Pap. Mag. Canada 62 (1), 39–48.
Haslach, H.W., 1994. Relaxation of moisture accelerated creep and hygroexpansion. In: Proceedings of the Moisture-Induced Creep Behavior of Paper and Board Conference, Stockholm, pp. 121–138.
Hill, R., 1948. A theory of the yielding and plastic flow of anisotropic metals. Proc. R. Soc. London Ser. A, Math. Phys. Sci. 191, 281–297.
Hoole, S.M., I'Anson, S.J., Ora, M., Ashworth, T.N., Briggs, D., Phillips, B., Hoyland, R.W., 1999. CD shrinkage profiles of paper – experiments on a commercial paper machine. Pap. Technol. 40 (10), 63–70.
Ivarsson, B.W., 1954. Introduction of stress into a paper sheet during drying. Tappi 37 (12), 634–639.
Johnson, M.W., Urbanik, T.J., 1984. A nonlinear theory for elastic plates with application to characterizing paper properties. J. Appl. Mech. 51, 146–152.
Johnson, M.W., Urbanik, T.J., 1987. Buckling of axially loaded, long rectangular paperboard plates. Wood Fiber Sci. 19 (2), 135–146.
Kijima, T., Yamakawa, I., 1978. Effect of shrinkage during drying on dimensional stability of paper. Jpn. Tappi J. 32 (10), 584–592.
Kiyoaki, I., 1987. The computer simulation on a web shrinkage in a paper machine dryer section. Part 1. Elastic modulus and drying force as a function of a web moisture. Japan. Tappi J. 41 (12), 1229–1234.

Kouko, J., Salminen, K., Kurki, M., 2007. Laboratory scale measurement procedure for the runnability of a wet web on a paper machine, part 2. Pap. Timber 89 (7–8), 424–430.
Kulachenko, A., Gradin, P., Uesaka, T., 2005. Tension wrinkling and fluting in heatset web offset printing process – post-buckling analysis. In: Proceedings of 13th Pulp and Paper Fundamental Research Symposium, Cambridge, pp. 1075–1099.
Land, C., Wahlström, T., Stolpe, L., 2008. Moisture streaks and their relation to baggy paper webs. J. Pulp Pap. Sci. 34 (4), 234–239.
Larsson, P.A., Wågberg, L., 2008. Influence of fibre–fibre joint properties on the dimensional stability of paper. Cellulose 15 (4), 515–525.
Lavrykov, S., Ramarao, B.V., Lyne, A.L., 2004. The planar transient hygroexpansion of copy paper: experiments and analysis. Nordic Pulp Pap. Res. J. 19 (2), 183–190.
Leppänen, T., Sorvari, J., Erkkilä, A.-L., Hämäläinen, J., 2005. Mathematical modelling of moisture induced out-of-plane deformation of a paper sheet. Model. Simul. Mater. Sci. Eng. 13, 841–850.
Leppänen, T., Erkkilä, A.-L., Hämäläinen, J., 2008. Effect of fiber orientation structure on simulated cockling of paper. Pulp Pap. Canada 109 (2), 31–38.
Lif, J.O., Fellers, C., Söremark, C., Sjödahl, M., 1995. Characterizing the in-plane hygroexpansivity of paper by electronic speckle microscope. J. Pulp Pap. Sci. 21 (9), 302–309.
Lif, J., Östlund, S., Fellers, C., 1999. Applicability of anisotropic viscoelasticity of paper at small deformations. Mech. Time Depend. Mater. 2 (3), 245–267.
Lif, J., Östlund, S., Fellers, C., 2005. In-plane hygro-viscoelasticity of paper at small deformations. Nordic Pulp Pap. Res. J. 20 (1), 139–149.
Lif, J.O., 2006. Hygro-viscoelastic stress analysis in paper web offset printing. Finite Elem. Anal. Des. 42 (5), 341–366.
Lipponen, P., Leppänen, T., Kouko, J., Hämäläinen, J., 2008. Elasto-plastic approach for paper cockling phenomenon: on the importance of moisture gradient. Int. J. Solids Struct. 45, 3596–3609.
Lipponen, P., Erkkilä, A.-L., Leppänen, T., Hämäläinen, J., 2009. On the importance of in-plane shrinkage and through-thickness moisture gradient during drying on cockling and curling phenomena. In: Proceedings of 14th Pulp and Paper Fundamental Research Symposium, Oxford, pp. 389–436.
Lu, W., Carlsson, L.A., 2001. Influence of viscoelastic behavior on curl of paper. Mech. Time Depend. Mater. 5, 79–100.
Lyne, L.M., Gallay, W., 1954. Fiber properties and fiber water relationships in relation to the strength and rheology of wet webs. Tappi 37 (12), 581–596.
Lyne, A., Fellers, C., Kolseth, P., 1996. The effect of filler on hygroexpansivity. Nordic Pulp Pap. Res. J. 11 (3), 152–163.
Manninen, M., Kajanto, I., Happonen, J., Paltakari, J., 2011. The effect of microfibrillated cellulose addition on drying shrinkage and dimensional stability of wood-free paper. Nordic Pulp Pap. Res. J. 26 (3), 297–305.
Mendes, A.H.T., Park, S.W., Ferreira, P.J.T., Almeida, F.S., 2011. Hygroexpansivity profiles on a commercial paper machine. Nordic Pulp Pap. Res. J. 26 (3), 312–318.
Mäkelä, P., Östlund, S., 2003. Orthotropic elastic–plastic material model for paper materials. Int. J. Solids Struct. 40, 5599–5620.
Mäkelä, P. 2009. Effect of drying conditions on the tensile properties of paper. In: Proceedings of 14th Pulp and Paper Fundamental Research Symposium, Oxford, pp. 1079–1094.
Nanko, H., Wu, J., 1995. Mechanisms of paper shrinkage during drying. In: Proceedings of International Paper Physics Conference (CPPA and Tappi), pp. 103–113.
Nanri, Y., Uesaka, T., 1993. Dimensional stability of mechanical pulps – drying shrinkage and hygroexpansivity. Tappi J. 76 (6), 62–66.
Nordman, L.S., 1958. Laboratory investigations into the dimensional stability of paper. Tappi 41 (1), 23–50.
Page, D.H., Tydeman, P.A., 1962. A new theory of the shrinkage, structure and properties of paper. In: Transactions of the Symposium on Formation and Structure of Paper, British Paper and Board Makers' Association, London, pp. 397–413.
Pecht, M.G., Johnson, M.W., Rowlands, R.E., 1984. Constitutive equations for the creep of paper. Tappi 67 (5), 106–108.
Pecht, M., Johnson, M.W., 1985. The strain response of paper under various constant regain states. Tappi 68 (1), 90–93.
Rance, H.F., 1954. Effect of water removal on sheet properties. Tappi 37 (12), 640–648.
Rance, H.F., 1956. The formulation of methods and objectives appropriate to the rheological study of paper. Tappi 39 (2), 104–115.
Rand, J.L., 1995. A nonlinear viscoelastic creep model. Tappi J. 78 (7), 178–182.
Roisum, D.R., 1996. The mechanics of wrinkling. Tappi J. 79 (10), 217–226.
Salmen, L., Fellers, C., Htun, M., 1987. The development and release of dried-in stresses in paper. Nordic Pulp Pap. Res. J. 2 (2), 44–48.
Setterholm, V., Kuenzi, E.W., 1970. Fiber orientation and degree of restraint during drying – effect of tensile anisotropy of paper handsheet. Tappi 53 (10), 1915–1920.
Silvy, J., 1971. Effects of drying on web characteristics. Pap. Technol. 12 (5), 377–387.
Skowronski, J., Robertson, A.A., 1986. The deformation properties of paper: tensile strain and recovery. J. Pulp Pap. Sci. 12 (1), 20–25.
Steenberg, B., 1947. Paper as a visco-elastic body. Svensk Papperstidning 50 (6), 127–140.
Strömbro, J., Gudmundson, P., 2008. Mechano-sorptive creep under compressive loading – a micromechanical model. Int. J. Solids Struct. 45 (9), 2420–2450.
Suhling, J.C., Rowlands, R.E., Johnson, M.W., Gunderson, D.E., 1985. Tensorial strength analysis of paperboard. Exp. Mech. 25 (1), 75–84.
Tydeman, P.A., Wembridge, D.R., Page, D.H. 1966. Transverse shrinkage of individual fibers by microradiography. In: Consolidation of the Paper Web: Transactions of the Symposium, Cambridge, pp. 119–144.
Uesaka, T., Murakami, K., Imamura, R., 1980. Two-dimensional linear viscoelasticity of paper. Wood Sci. Technol. 14, 131–142.
Uesaka, T., Kodaka, I., Okushima, S., Fukuchi, R., 1989. History-dependent dimensional stability of paper. Rheol. Acta 28, 238–245.
Uesaka, T., 1991. Dimensional stability of paper – upgrading paper performance in end use. J. Pulp Pap. Sci. 17 (2), 39–46.
Uesaka, T., Moss, C., Nanri, Y., 1992. The characterisation of hygroexpansivity of paper. J. Pulp Pap. Sci. 18 (1), 11–16.
Uesaka, T., 1994. General formula for hygroexpansion of paper. J. Mater. Sci. 29 (9), 2373–2377.
Uesaka, T., Qi, D., 1994. Hygroexpansivity of paper: effects of fibre-to-fibre bonding. J. Pulp Pap. Sci. 20 (6), 175–179.
Urbanik, T.J., 1995. Hygroexpansion-creep model for corrugated fiberboard. Wood Fiber Sci. 27 (2), 134–140.
Wahlström, T., Adolfsson, K., Östlund, S., Fellers, C. 1999. Numerical modelling of the cross direction shrinkage profile in a drying section: a first approach. In: Proceedings of the 1999 TAPPI International Paper Physics Conference, San Diego, California, pp. 517–531.
Wahlström, T., Fellers, C., 2000. Biaxial straining of handsheets during drying – effects on in-plane mechanical properties. Tappi J. 83 (8), 1–8.
Wahlström, T., Lif, J.O., 2003. Dryer section simulator for laboratory investigations of shrinkage profile. In: Proceedings of International Paper Physics Conference (PAPTAC), pp. 169–173.
Wahlström, T., 2004. Development of paper properties during drying. Pap. Prod. Phys. Technol., 69–107
Xia, Q.S., Boyce, M.C., Parks, D.M., 2002. A constitutive model for the anisotropic elastic–plastic deformation of paper and paperboard. Int. J. Solids Struct. 39, 4053–4071.
Yeh, K.C., Considine, J.M., Suhling, J.C., 1991. The influence of moisture content on the nonlinear constitutive behavior of cellulosic materials. In: Tappi Proceedings: 1991 International Paper Physics Conference, Tappi, pp. 695–711.
Östlund, M., Östlund, S., Carlsson, L.A., Fellers, C., 2004. The influence of drying restraints and beating degree on residual stress build-up in paperboard. J. Pulp Pap. Sci. 30 (11), 289–292.
Östlund, M., 2006. Modeling the influence of drying conditions on the stress buildup during drying of paperboard. J. Eng. Mater. Technol. Trans. ASME 128 (4), 495–502.